Gating Consequences of Charge Neutralization of Arginine Residues in the S_4 Segment of $K_v7.2$, an Epilepsy-Linked K^+ Channel Subunit

Francesco Miceli,* Maria Virginia Soldovieri,* Ciria C. Hernandez,† Mark S. Shapiro,† Lucio Annunziato,* and Maurizio Taglialatela*‡

*Section of Pharmacology, Department of Neuroscience, University of Naples Federico II, Naples 80131, Italy; †Department of Physiology, University of Texas Health Science Center, San Antonio, Texas 77229; and ‡Department of Health Science, University of Molise, Campobasso, Italy

ABSTRACT The $K_v7.2$ subunits are the main molecular determinants of the M-current, a widespread K^+ current regulating neuronal excitability. Mutations in the *$K_v7.2$* gene cause benign familial neonatal seizures, an autosomally inherited human epilepsy. The benign familial neonatal seizure-causing mutations include those at arginine residues at positions 207 and 214 in the S_4 segment of $K_v7.2$. In this study, each of the six S_4 arginines was individually replaced with neutral glutamines, and the functional properties of mutant channels were studied by whole-cell and single-channel voltage-clamp measurements. The results obtained suggest that each S_4 arginine residue plays a relevant role in the voltage-dependent gating of $K_v7.2$ channels. In particular, a decreased positive charge at the N-terminal end of S_4 stabilized the activated state of the voltage-sensor, whereas positive-charge neutralization at the C-terminal end of S_4 favored the resting conformation. Strikingly, neutralization of a single arginine at position 201 was sufficient to cause a significant loss of voltage dependence in channel activation. Moreover, by comparing the functional properties of glutamine versus tryptophan substitution, we found steric bulk to play a relevant role at position 207, but not at position 214, in which the main functional effect of this disease-causing mutation seems to be a consequence of the loss of the positive charge.

INTRODUCTION

Potassium (K^+) currents play critical roles in a wide range of physiological processes such as the propagation of electrical signals by nerve cells, muscle contraction, cell volume regulation, and secretion of hormones and neurotransmitters (1). A wide variety of K^+ currents has been described, each showing distinct tissue distribution and subcellular localization, often with peculiar biophysical, pharmacological, and modulatory properties. Several factors are involved in generating such extraordinary functional heterogeneity; the primary factor involves the large diversity in genes encoding for K^+ channel subunits.

In voltage-gated K^+ channels (K_v channels), which represent the largest family of K^+ channels, specific conformational transitions triggered by membrane potential changes regulate the probability of channel opening. The K_v channels assemble as tetramers of identical or compatible subunits, each containing six transmembrane segments (S_1–S_6). Within each subunit, the S_5–S_6 domain contributes to the formation of the ion-selective pore and the inner pore gate, whereas the S_1–S_4 region forms the voltage sensor domain (VSD).

The recently solved structure of three bacterial nonvoltage-gated K^+ channels, KcsA (2), MthK (3,4), and KirBac1.1 (5), whose membrane core of each subunit only contains the regions corresponding to the S_5–S_6 domain and the intervening linker, has provided a valuable structural model to explain the molecular mechanisms of ion permeation, selectivity, and pore opening/closing behavior. In K_v channel subunits, pore opening is controlled by the VSD domain. Within this region, a critical gating role has traditionally been assigned to the S_4 segment that contains several positively charged residues spaced by mostly hydrophobic residues, and whose movement through the membrane electric field appears to represent the first gating transition in response to changes in membrane voltage (6,7). The crystal structure of the first voltage-gated K^+ channel subunits containing six transmembrane segments including a VSD, i.e., the bacterial K_vAP (8) and the mammalian $K_v1.2$ (9,10), seems to support such a view, although the intimate details of such movement, including the position of the VSD in the closed-channel configuration, the extent of VSD dislocation during activation (ranging from 2 Å to 15–20 Å), the relative role of the hydrophobic membrane interface, and the coupling of such movement to the inner pore gate, remain highly controversial (11).

Because of their fundamental role in regulating cellular excitability and ion distribution across the plasma membrane, K_v channels are implicated in several human disease conditions, including epilepsy, pain, migraine, arrhythmias, sensory dysfunction, and metabolic illnesses. In particular, mutations in four of the five members of the *K_v7* gene family (*$K_v7.1$–$K_v7.5$*) were associated with human channelopathies. Thus, gene defects affecting $K_v7.1$, which is mainly expressed in the heart, gastrointestinal epithelia, and inner ear, but not in the brain, are responsible for the chromosome 11-linked form of long QT syndrome, whereas those targeting $K_v7.4$ were found in families affected by a rare form of

Submitted December 27, 2007, and accepted for publication May 6, 2008.

Address reprint requests to Maurizio Taglialatela, Division of Pharmacology, Dept. of Neuroscience, School of Medicine, University of Naples Federico II, Ed. 19, Via Pansini 5, 80131 Naples, Italy. Tel.: 39-081-7463310/3318; Fax: 39-081-7463323; E-mail: mtaglial@unina.it.

Editor: Toshinori Hoshi.

0006-3495/08/09/2254/11 $2.00

doi: 10.1529/biophysj.107.128371

nonsyndromic autosomal-dominant hearing loss (DFNA2). Mutations in *$K_v7.2$* and more rarely *$K_v7.3$* genes were identified in families affected by an autosomally dominantly inherited epilepsy of the newborn defined as benign familial neonatal seizures (BFNS). Neuron-specific $K_v7.2$ and $K_v7.3$ subunits can form either homomeric or heteromeric K^+ channels underlying the so-called M-current (I_{KM}) (12), a K^+ current which regulates neuronal excitability, functioning as a brake for repetitive action potential firing and as a major determinant of spike frequency adaptation (13). It is widely thought that mutation-induced reduction in I_{KM} function can increase neuronal excitability, leading to epileptic phenotypes. Consequently, I_{KM} is regarded as a primary target for pharmacological intervention against hyperexcitability diseases (14,15).

Disease-causing mutations often indicate functionally relevant domains in the proteins affected. In $K_v7.2$, most BFNS-causing mutations are localized either in the large C-terminal domain, a critical region for subunit assembly and channel regulation by intracellular molecules, and in the VSD. In the VSD, mutations causing the substitution of two arginine (R) residues at positions 207 and 214 with tryptophan (W) were described in BFNS patients, highlighting their key role in $K_v7.2$ subunit function (16,17).

In this study, mutagenesis, macroscopic and single-channel electrophysiology, and molecular modeling experiments were performed to evaluate the role of each of the six R residues present in the S_4 segment in the gating of $K_v7.2$ channels, by replacing them individually with neutral glutamines (Q). Moreover, to clarify the possible role of steric bulk of the residues introduced at positions 207 and 214 in BFNS pathogenesis, the properties of the channels carrying smaller Q residues at positions 207 and 214 were compared with those of channels in which the same positions were occupied by bulkier W residues.

MATERIALS AND METHODS

Mutagenesis and heterologous expression of $K_v7.2$ cDNAs

Mutations were engineered in human $K_v7.2$ cDNA (cloned into pcDNA3.1) by sequence overlap extension polymerase chain reaction (PCR), using Pfu DNA polymerase, as previously described (17). After PCR, mutation-containing fragments were cloned into $K_v7.2$, using *Not*I and *Pml*I restriction enzymes. All sequences were verified with the Big Dye Terminator Cycle Sequencing Kit in an ABI Prism 310 automated sequencer (Applied Biosystems, Foster City, CA). Wild-type (wt) and mutant cDNAs were expressed in Chinese hamster ovary (CHO) cells by transient transfection. The CHO cells were grown in 100-mm plastic petri dishes in DMEM containing 10% fetal bovine serum, nonessential amino acids (0.1 mM), penicillin (50 U/mL), and streptomycin (50 μg/mL) in a humidified atmosphere at 37°C with 5% CO_2. For electrophysiological experiments, cells were seeded on glass coverslips (Carolina Biological Supply Company, Burlington, NC) and transfected the next day, using Lipofectamine 2000 (whole-cell recordings; Invitrogen, Milan, Italy) or Polyfect (single-channel recordings; Qiagen, Valencia, CA), according to the manufacturer's protocols. A plasmid encoding for enhanced green fluorescent protein (Clontech, Palo Alto, CA) was used as a transfection marker, with total cDNA in the transfection mixture kept constant at 4 μg.

Whole-cell electrophysiology

Currents from CHO cells were recorded at room temperature (20–22°C) 1 day after transfection, with an Axopatch 200A (Molecular Devices, Union City, CA), using the whole-cell configuration of the patch-clamp technique, with glass micropipettes of 3–5 MΩ resistance. The extracellular solution contained (in mM): 138 NaCl, 2 $CaCl_2$, 5.4 KCl, 1 $MgCl_2$, 10 glucose, and 10 HEPES, pH 7.4, with NaOH. The pipette (intracellular) solution contained (in mM): 140 KCl, 2 $MgCl_2$, 10 EGTA, 10 HEPES, 5 Mg-ATP, 0.25 cAMP, pH 7.3–7.4, with KOH. We used pCLAMP software (version 6.0.4, Molecular Devices) for data acquisition and analysis. To generate conductance/voltage (G/V) curves, cells were held at −80 mV and then depolarized for 3 s from −80 to +20/+70 mV in 10-mV increments, followed by an isopotential pulse at 0 mV of 350-ms duration. Current values recorded at the beginning of the 0-mV pulse were normalized and expressed as a function of the preceding voltages. The data were fit to a Boltzmann equation of the following form: $y = max/[1 + exp(V_{1/2} - V)/k]$, where V is the test potential, $V_{1/2}$ is the half-activation potential, and k is the slope factor. To analyze current-activation kinetics, the current traces recorded in response to incremental voltage steps were fitted to a single-exponential function of the following form: $y = amp\ exp(-t/\tau) + c$, where *amp* indicates the amplitude of the exponential component, and τ indicates the time constant. The tetraethylammonium (TEA) blockade was quantified by measuring the percentage of current inhibition at 0 mV produced by a 2-min drug application.

Single-channel electrophysiology

For single-channel recordings, channel activity in cell-attached patches was measured 48–96 h after transfection. Pipettes had resistances of 7–15 MΩ when filled with a solution that contained (in mM): 105 NaCl, 50 KCl, 2 $CaCl_2$, 1 $MgCl_2$, and 10 HEPES, pH 7.4, with NaOH. Cells were bath-perfused with a solution containing (in mM): 175 KCl, 4 $MgCl_2$, and 10 HEPES, pH 7.4, with KOH. This high (K^+) solution served to clamp the resting membrane potential near 0 mV. Recording and analysis methods were similar to those described previously (18,19). Currents were recorded using an Axopatch 1-D amplifier (Molecular Devices). The data were acquired using Pulse software (HEKA Electronik, Lambrecht, Germany), sampled at 5 kHz, and filtered at 500 or 200 Hz. Single-channel data were analyzed using PulseFit and TAC (Bruxton, Seattle, WA). Open and closed events were analyzed using the ''50% threshold criterion.'' All events were carefully checked visually before being accepted. Open probability (p_o) histograms were generated using TACFit (Bruxton). The total number of channels in a given patch was estimated on the basis of two common assumptions: 1), that all of the channels in a patch behaved in an identical manner, i.e., they were homogeneous; and 2), that the P_o of one channel did not depend on the gating state of the other(s), i.e., they were independent. Under these assumptions, only one channel in the patch was considered to be present if no superimposed openings were observed for a sufficiently long period of time that depended on the P_o of any given channel. In the case of multiple channels in the patch, the number of open channels was governed by the binomial distribution (20). In our case, we evaluated the total number of channels in the patch by continuously recording for >1 min at strongly depolarized potentials, at which P_o was the highest (~0.2). Using this method, we estimated a maximal error rate of 3.8%, which is within the error of the pooled measurements. When superimposed openings were observed, the total number of channels in the patch was estimated from the maximal number of superimposed openings. At any given potential, the single-channel amplitude (i) was calculated by fitting all-point histograms with single or multi-Gaussian curves. The difference between fitted ''closed'' and ''open'' peaks was taken as i. Distributions of open and closed times were logarithmically binned and fitted with exponential densities by the method of

maximum likelihood, as previously described (18). Single-channel conductance was calculated from the slope of the I/V chord fitted by linear regression, using GraphPad Prism version 4.0 for Windows (GraphPad Software, San Diego, CA).

Homology modeling

Three-dimensional models of wt and mutant $K_v7.2$ subunits were generated by homology modeling, using known structures of K_v channel subunits available in the Protein Data Bank (PDB), using SWISS-MODEL, a program that performs automated sequence-structure comparisons (21). The model generated was analyzed using both the DeepView module of the Swiss-PDBViewer (version 3.7, available at http://www.expasy.ch/spdbv/) and PyMOL (available at http://pymol.sourceforge.net/).

The $K_v7.2$ subunit sequence showed homology with a recently described chimeric channel in which the voltage-sensor paddle (corresponding to the S_{3b}–S_4 region) of $K_v2.1$ was transferred into the Kv1.2 subunit (22) (PDB accession number 2R9RH; 29% of sequence identity) and to $K_v1.2$ (10) (PDB accession number 2A79B; 26% of sequence identity). In this study, the homology model was built using the 2R9RH structure as template.

Statistics

Data are expressed as mean ± SE. Statistically significant differences between data were evaluated using Student's *t* test.

RESULTS

Biophysical properties of $K_v7.2$ channels carrying neutralizations in S_4 arginines

The upper panel of Fig. 1 shows a schematic representation of a single $K_v7.2$ subunit, indicating the six transmembrane segments, the intervening linkers, and the intracellular N and C termini. An alignment of the primary sequence of S_4 and surrounding regions of all K_v7 family members and other K^+ channel subunits is shown in the lower part of Fig. 1, revealing a variable number of positive charges, ranging from seven in *Shaker*, six in $K_v7.2$–7.5 channels, and only four in $K_v7.1$ subunits. Each of the six charged arginine residues is numbered from R1 to R6 according to their relative position in the linear sequence. For $K_v7.2$, the six R residues corresponded to residues R198, R201, R207, R210, R213, and R214. In all K_v7 subunits, the positively charged R corresponding to position 204 in $K_v7.2$, which is located in the middle of the S_4 segment and is highly conserved in most ion channel subunits, is replaced by an uncharged Q residue. To investigate the relative contribution of each S_4 R residue in $K_v7.2$ voltage-dependent gating, we engineered mutant constructs in which each of the six R residues was replaced with Q, thus generating the mutant subunits which were named R1Q, R2Q, R3Q, R4Q, R5Q, and R6Q (corresponding to the mutations R198Q, R201Q, R207Q, R210Q, R213Q, and R214Q, respectively). These constructs were expressed in CHO cells, and the functional properties of the channels generated were measured using the whole-cell configuration of the patch-clamp technique.

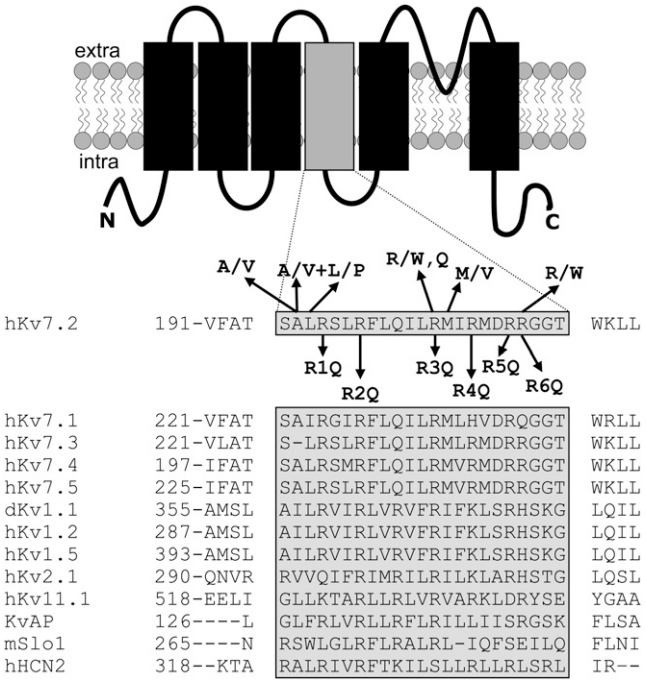

FIGURE 1 Schematic topology of a $K_v7.2$ subunit and sequence alignment of the S_4 region among voltage-gated K^+ channels. Shaded area corresponds to the S_4 sequence. On top of the $K_v7.2$ sequence, amino-acid substitutions associated with BFNS are shown. Below the $K_v7.2$ sequence are the positions and nomenclatures of the mutations investigated.

Cells heterologously expressing homomeric $K_v7.2$ subunits ($wtK_v7.2$) displayed voltage-dependent, K^+-selective currents characterized by a rather slow time course of activation and deactivation, and a threshold for current activation around −60 mV (Fig. 2). When conditioning depolarizing pulses from −80 mV to +20 mV were followed by an isopotential test pulse to 0 mV (as described in Materials and Methods), the instantaneous current amplitude of the test pulse was saturated at 0 mV. Heterologous expression of all homomeric $K_v7.2$ subunits carrying the indicated mutations in S_4 yielded currents comparable in size to the currents recorded from cells expressing $wtK_v7.2$ channels. The current density, expressed in pA/pF, and measured at potentials in which the conductance was saturated (+20/+70 mV, see below), was 50 ± 6, 35 ± 12, 46 ± 12, 47 ± 8, 40 ± 10, 41 ± 13, and 33 ± 7 for $wtK_v7.2$, R1Q, R2Q, R3Q, R4Q, R5Q, and R6Q, respectively (n = 6–18). As expected, all of the mutant channels retained their selectivity for K^+ over Na^+ ions. Using standard intracellular and extracellular recording solutions (see Materials and Methods), the current reversal potentials (expressed in mV) were −78 ± 1, −76 ± 1, −79 ± 1, −77 ± 1, −75 ± 1, −75 ± 1, and −79 ± 1, for $wtK_v7.2$, R1Q, R2Q, R3Q, R4Q, R5Q, and R6Q, respectively (n = 3–8).

The voltage dependence of activation was markedly affected in $K_v7.2$ channels carrying the neutralization of each of the S_4 R residues (Fig. 2). In particular, when compared to

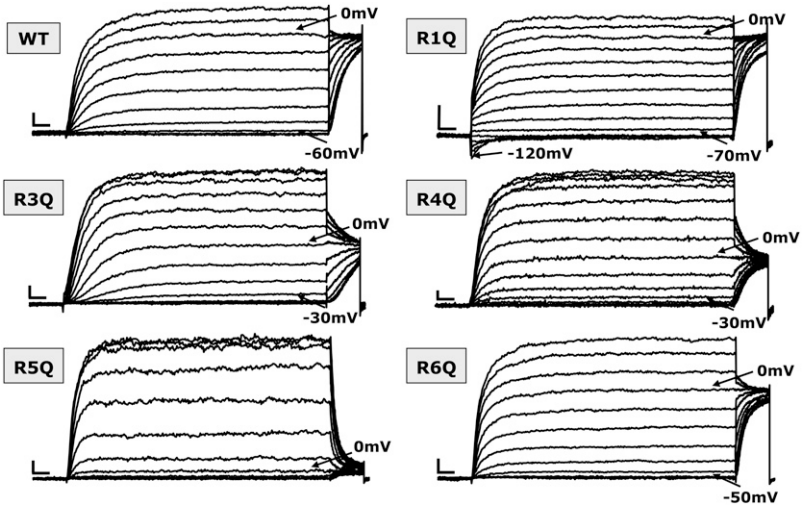

FIGURE 2 Representative current traces of wt and R1Q, R3Q, R4Q, R5Q, and R6Q $K_v7.2$ mutants expressed in CHO cells. Each family of currents was recorded from a different cell held at −80 mV and then depolarized for 3 s from −120 to +20/+70 mV in 10-mV increments, followed by an isopotential pulse at 0 mV of 350-ms duration. For each set of recordings, arrows indicate current traces corresponding to the threshold potential and the 0-mV pulse. Current scale, 200 pA; timescale, 0.2 s.

wt channels, the currents carried by the R1Q mutant $K_v7.2$ channels activated at lower membrane potentials, and were already significantly activated at the holding potential of −80 mV. In fact, hyperpolarizing pulses from −80 mV to −120 mV caused the R1Q channels to deactivate, generating inwardly directed currents that relaxed toward zero. Moreover, during the isopotential test pulse to 0 mV that followed the conditioning pulses from −120 mV to +20 mV, the instantaneous currents saturated at conditioning pulses below −20 mV. On the other hand, homomeric R3Q, R4Q, R5Q, and R6Q channels displayed currents with more positive activation thresholds. The R5Q mutant displayed the most dramatic effect, whereas the R6Q mutant was only slightly different from wt$K_v7.2$ channels.

To quantify the relative changes prompted by each of the S_4 mutations on the voltage dependence of the activation of $K_v7.2$ channels, we plotted the normalized current amplitudes at the start of the 0-mV isopotential pulse as a function of membrane potential (Fig. 3 *A*). These data were fit to a Boltzmann equation to obtain the half-activation potential ($V_{1/2}$; Fig. 3 *B*) and the slope factor (k; Fig. 3 *C*) for each channel type. The resulting $V_{1/2}$ values (expressed in mV) were −39.5 ± 1.2, −66.0 ± 2.3, −16.9 ± 2.7, 0.0 ± 3.6, 24.8 ± 3.1, and −5.5 ± 1.7, for channels composed of wt, R1Q, R3Q, R4Q, R5Q, and R6Q $K_v7.2$ subunits, respectively. The k values (expressed as mV/e-fold) were: 10.7 ± 0.6, 13.4 ± 0.7, 11.3 ± 0.6, 16.9 ± 1.0, 13.1 ± 0.9, and 13.3 ± 1.0, for channels composed of wt, R1Q, R3Q, R4Q, R5Q, and R6Q $K_v7.2$ subunits, respectively. Collectively, these results suggest that each of the R residues in the $K_v7.2$ S_4 segment plays an important role in channel gating. In particular, neutralization of the R1 residue located at the N-terminal end of S_4 caused a hyperpolarizing shift in the voltage dependence of activation, whereas neutralization of the R3, R4, R5, and R6 residues, positioned toward the C-terminal end of the S_4 segment, caused gating changes in the opposite direction, i.e., a positive shift of the voltage dependence of activation.

Removal of the charge at the R2 position in S_4 causes a marked loss of voltage-dependent gating in $K_v7.2$ channels

The S_4 mutants described so far displayed varying shifts in the voltage dependence of activation, but all still behaved qualitatively similar to wt$K_v7.2$ channels. However, the replacement of the R2 residue with a glutamine residue (R2Q) unexpectedly yielded channels that displayed a significant loss of time-dependent kinetics (Fig. 4 *A*). The R2Q channels behaved as K^+-selective leak channels that were largely open at all test potentials. Indeed, the recorded R2Q currents had a reversal potential of a K^+-selective pore (−79 ± 1 mV). When the normalized current amplitudes, measured at the end of test pulses from −120 mV to +40 mV, were plotted against the membrane potential for R2Q $K_v7.2$ channels, the I/V was completely linear within the potential range from −120 mV to −20 mV, suggesting that the channels carrying the R2Q mutation largely lost their voltage-dependent gating (Fig. 4 *B*). Using the same protocol, the normalized I/V of wt$K_v7.2$ channels failed to show an inward current component at potentials more negative than −60 mV, because of the strong tendency of channels to close at such potentials (Fig. 4 *B*). A slight inward rectification of the I/V relationship, suggestive of a decrease in conductance at depolarizing pulses more positive than −20 mV, was observed for R2Q channels (Fig. 4 *A*), and was similarly observed in wt$K_v7.2$ channels studied at the macroscopic or single-channel level (18,19).

To estimate the fraction of the current displaying slow time-dependent activation at depolarizing voltages in R2Q channels, we measured the current amplitudes at the beginning (A_1, Fig. 4 *A*) and end (A_2, Fig. 4 *A*) of the 0-mV pulse

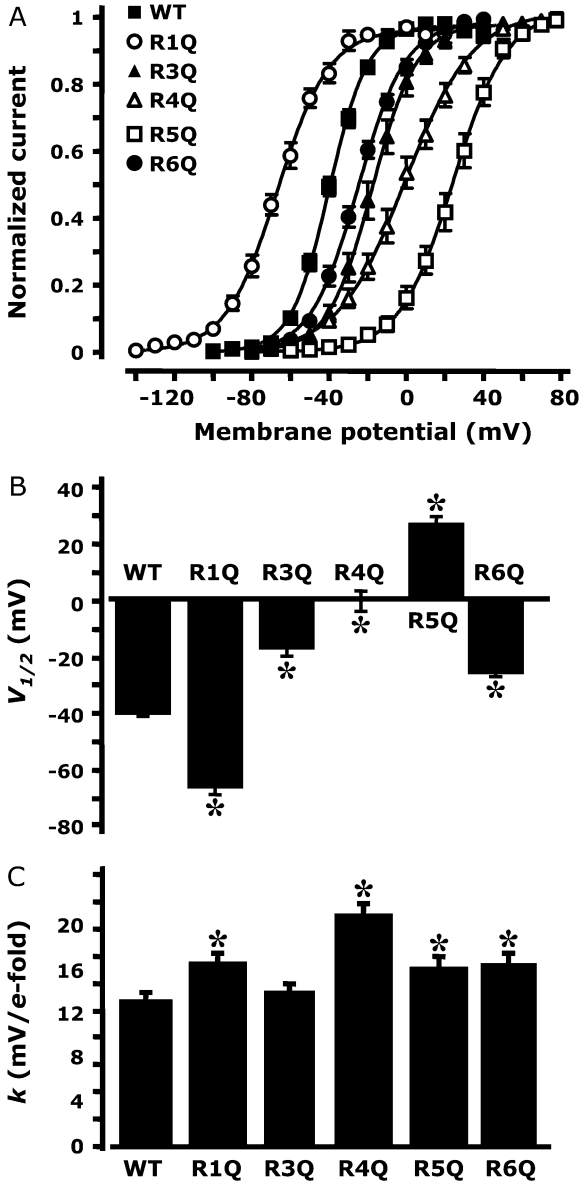

FIGURE 3 Analysis of gating properties of wt and R1Q, R3Q, R4Q, R5Q and R6Q $K_v7.2$ channels. (*A*) Steady-state activation curves, obtained by plotting normalized currents at the beginning of the 0-mV pulse as a function of the preceding conditioning potential. Continuous lines represent Boltzmann fits of the experimental data. $V_{1/2}$ (expressed in mV, *B*) and *k* (expressed in mV/*e*-fold, *C*) values obtained for each indicated channel from the analysis of the data in *A*. *Values significantly different ($p < 0.05$) from the corresponding value of wt$K_v7.2$ channels.

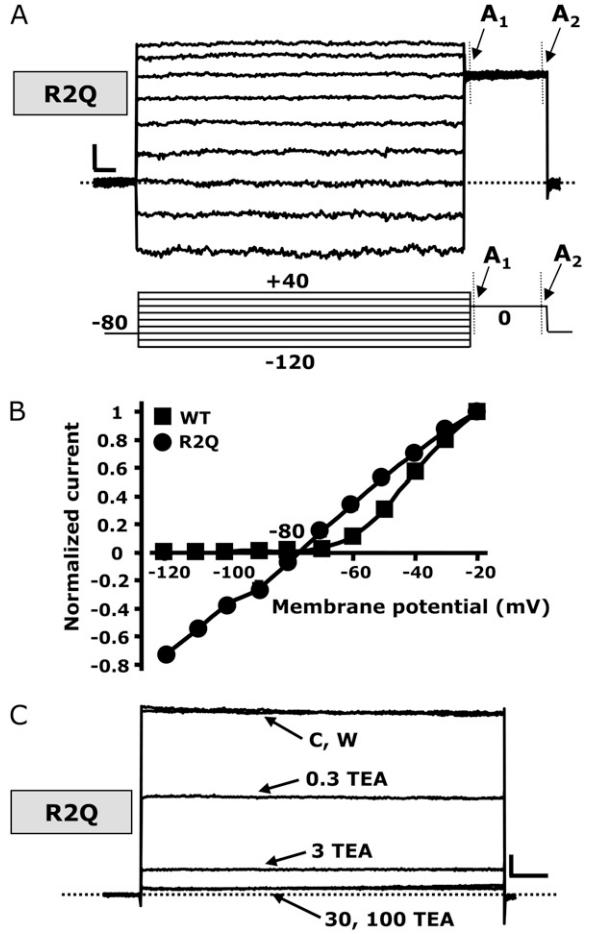

FIGURE 4 Biophysical and pharmacological properties of mutant R2Q $K_v7.2$ channels. (*A*) Representative current traces recorded using a voltage protocol in which the cell was held at −80 mV and then depolarized for 1.5 s from −120 to +40 mV in 20-mV increments, followed by an isopotential pulse at 0 mV of 350-ms duration. Below the traces is a schematic drawing of the voltage pulse protocol applied. A_1 and A_2 values refer to the beginning and end of 0-mV pulses, where current amplitudes were measured to calculate the time-dependent component (A_2–A_1/A_2). (*B*) Plot of instantaneous currents normalized at the value obtained at −20 mV for both wt (*squares*, n = 20) and R2Q (*circles*, n = 10) $K_v7.2$ channels. (*C*) Currents from CHO cells expressing R2Q $K_v7.2$ channels were recorded using 2-s voltage steps to 0 mV, delivered at a frequency of 0.1 Hz from a holding voltage of −80mV. As indicated, the cell was sequentially exposed to control solution (*C*) and to 0.3, 3, 30, and 100 mM TEA_e (each for ~2 min), followed by washout (*W*). In both *A* and *C*, the current scale is 100 pA, and the timescale is 0.1 s.

(350-ms duration), delivered after prepulses to −120 or −100 mV. When averaging these values from several cells, we found the A_2–A_1/A_2 ratio to be 9.1% ± 1.0% (n = 4) and 6.9% ± 1.1% (n = 18) of the total current, respectively. This result suggested that a rather small fraction of the R2Q macroscopic current retained time-dependent kinetics; more than 90% of the macroscopic current between −120 mV and 0 mV appeared to be completely time-independent. We were unable to verify whether hyperpolarizing pulses more negative than −120 mV caused further R2Q channel deactivation because of the poor patch stability after long pulses at these negative voltages.

To confirm that these time-independent currents were carried by mutant R2Q $K_v7.2$ channels, we tested their sensitivity to the pore-blocker tetraethylammonium, applied extracellularly (TEA_e). Homomeric wt$K_v7.2$ channels are highly sensitive to TEA_e (12). Perfusion with increasing concentrations of TEA_e (0.3–100 mM) caused a similar dose-dependent and reversible blockade of currents in cells

expressing wt or R2Q $K_v7.2$ channels (Fig. 4 *C*). The percentage of current blocked at 0 mV in homomeric wt and R2Q $K_v7.2$ channels was 63% ± 9% and 57% ± 3%, respectively, using 0.3 mM TEA_e, and 89% ± 2% and 88% ± 2%, respectively, using 3 mM TEA_e (n = 5). The similar TEA_e sensitivity of wt and R2Q mutant $K_v7.2$ channels strongly suggested that the observed time- and voltage-independent currents are effectively carried by mutant R2Q $K_v7.2$ channels, and that the mutation did not affect the pore properties of these channels.

Given the dramatic gating changes observed in macroscopic current recordings from R2Q $K_v7.2$ channels, we performed single-channel measurements to evaluate the effects of the mutation on channel p_o and opening/closing kinetics as a function of voltage, as well as on single-channel conductance. To this end, we used the cell-attached configuration to avoid possible perturbations of the intracellular milieu, and to retain intact the biochemical machinery required for channel modulation (23). We used a pipette (extracellular) solution containing 50 mM K^+ to shift the equilibrium potential for K^+ ions to about −30 mV, allowing us to measure both inward and outward currents, using pulse or ramp protocols from hyperpolarized (−100/−80 mV) to depolarized (0/+40 mV) potentials.

Figure 5 *A* shows representative recordings obtained from wt and R2Q $K_v7.2$ channels, both using ramp (Fig. 5, *top*) and pulse (Fig. 5, *bottom*) voltage protocols. When the membrane voltage was ramped from −100 mV to +40 mV, openings of wt$K_v7.2$ channels were only detected in the outward direction (above −30 mV). In contrast, openings of R2Q channels were recorded throughout the entire voltage range, in both the inward and outward directions, according to changes in the driving force predicted for membrane potential. Similar results were also obtained using pulses to −80 mV or 0 mV. The p_o of wt$K_v7.2$ channels was unmeasurable at −80 mV (because no openings were detected), and reached a maximal value of 0.17 ± 0.01 (n = 14) at a depolarized potential of 0 mV. Consistent with previous work (18,19), such p_o values did not increase with further membrane depolarization (data not shown). Interestingly, the p_o recorded at 0 mV from the R2Q mutant $K_v7.2$ channel was similar to that obtained from wt channels at the same potential. Moreover, we were unable to detect statistically significant differences in p_o values measured between −80 mV or 0 mV in R2Q mutant $K_v7.2$ channels (Fig. 5 *B*), a result consistent with the marked loss of voltage dependence observed in macroscopic current recordings within the same voltage range. Kinetic analysis of homomeric $K_v7.2$ channels, similar to heteromeric $K_v7.2/K_v7.3$ channels and native I_{KM}, suggest the presence of at least three shut and two open states (18). The distributions of shut and open times obtained from single R2Q mutant $K_v7.2$ channels was also adequately fitted by

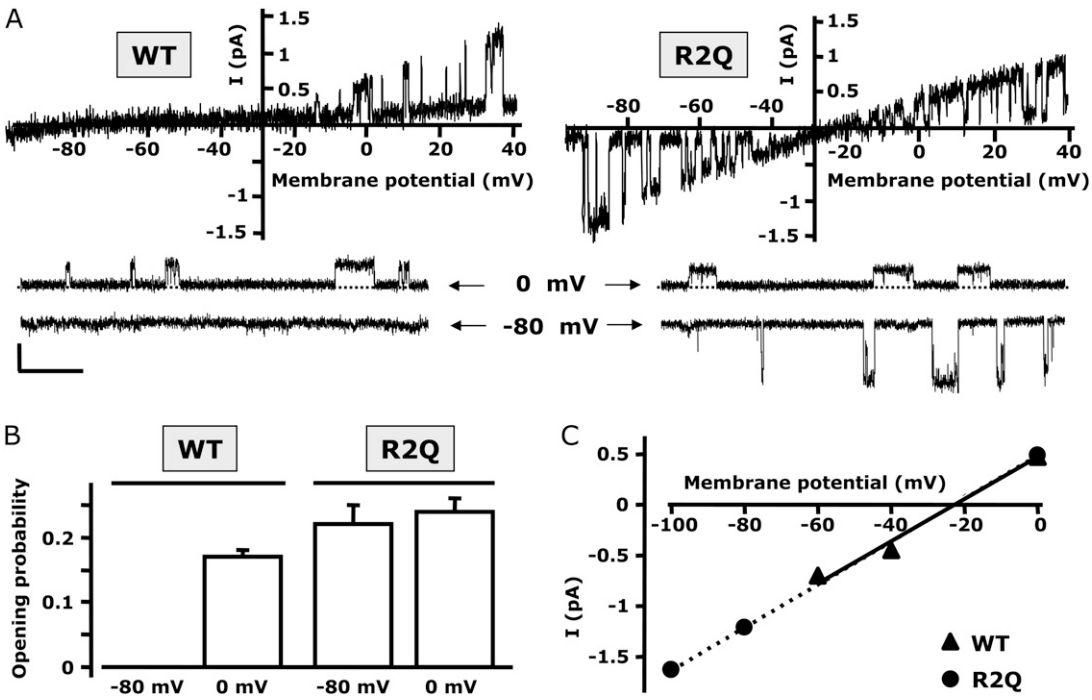

FIGURE 5 Single-channel properties of wt and R2Q $K_v7.2$ channels. (*A*, top) Representative single-channel traces recorded using a ramp voltage protocol (from −100 mV to + 40 mV; 3-s duration). (*Bottom*) representative single-channel sweeps obtained using pulses to the indicated potentials (−80 mV and 0 mV). (*B*) Plot of open probability obtained at −80 mV and 0 mV, as indicated (n = 8–14 patches for each data set). (*C*) Plot of unitary current-voltage relationships of single wt and R2Q $K_v7.2$ channels. Straight lines represent linear fits of experimental data. Each data point derives from the analysis of 5–7 patches. Current scale, 0.5 pA; timescale, 0.5 s.

three and two exponentials, respectively, at both −80 mV and 0 mV of membrane potentials. As shown in Table 1, the time constants for each of the three closed states (τ_{c1}, τ_{c2}, and τ_{c3}) and the two open states (τ_{o1} and τ_{o2}), as well as their relative contributions, were unaltered between −80 and 0 mV, again supporting the dramatic loss of channel voltage dependence observed for $K_v7.2$ R2Q channels within this voltage range.

Finally, despite these marked changes in voltage dependence of p_o, single-channel K^+ conductance was not affected by the mutation, at 20.8 ± 1.2 pS and 21.2 ± 0.4 pS for wt and R2Q $K_v7.2$ channels, respectively (n = 6), further arguing against a significant effect of the mutation on the conduction pathway of the $K_v7.2$ channel (Fig. 5 *C*).

Comparison between functional properties of $K_v7.2$ channels carrying glutamine-substituted R3 or R6 residues and those of tryptophan substitutions at the same positions

The S_4 region in $K_v7.2$ is a ''hot spot'' for mutations responsible for BFNS. In fact, both uncharged and charged substitutions were identified in several families affected by the disease; these are indicated above the sequence alignment shown in Fig.1 *A*. In particular, Dedek et al. (16) described the substitution of the R3 residue with a tryptophan (W) in a family affected by an unusual association of BFNS and neuromuscular abnormalities (myokymia). In another BFNS family, Castaldo et al. (17) found a mutation involving the R to W replacement at position R6. In addition, while this work was in preparation, a family affected by peripheral-nerve excitability (but not BFNS) that carried the R3Q mutation in $K_v7.2$ was described (24). To ascertain whether the previously described functional consequences introduced in $K_v7.2$ channels by the R3Q and R6Q mutations are only related to the loss of the positive charge of the R residue or to the specific properties of the side chains of the R-replacing amino acid, we compared the properties of the macroscopic currents of Q-substituted (R3Q and R6Q) and W-substituted (R3W and R6W) R3 or R6 residues in $K_v7.2$ channels, using the whole-cell configuration of the patch-clamp technique.

TABLE 1 $K_v7.2$ R201Q single-channel kinetics

Parameters	0 mV	−80 mV
τ_{c1} (ms)	4.9 ± 0.6	4.2 ± 0.4
Fraction (%)	30.5 ± 3.5	32.3 ± 2.3
τ_{c2} (ms)	30.6 ± 4.1	32.8 ± 4.5
Fraction (%)	37.6 ± 8.7	35.4 ± 5.4
τ_{c3} (ms)	250.6 ± 11.7	306.1 ± 37.4
Fraction (%)	31.9 ± 3.6	32.3 ± 5.4
τ_{o1} (ms)	7.9 ± 1.1	5.3 ± 0.6
Fraction (%)	40.9 ± 2.4	45.9 ± 5.0
τ_{o2} (ms)	59.1 ± 8.4	55.9 ± 11.1
Fraction (%)	59.1 ± 2.4	54.1 ± 5.0
i (pA)	0.54 ± 0.07	1.17 ± 0.08
n	7	9

Data are mean ± SE.

The results suggest that significant differences exist when $K_v7.2$ channels carrying the R3Q and the R3W substitutions are compared, with respect to both activation kinetics and steady-state properties. Although both substitutions caused a depolarizing shift in the midpoint potentials ($V_{1/2}$) of steady-state activation, the effect was more dramatic when the R3 position was occupied by a W compared with the R3Q substitution (Fig. 6). Moreover, the activation kinetics were very different. The fitting of current traces recorded at +20 mV to a single exponential function yielded activation time constants of 100 ± 4 ms for wt, 255 ± 42 ms for R3Q, and 1166 ± 260 for Q3W $K_v7.2$ channels (n = 5). These results clearly suggest that, at position R3, both charge and side-chain size influence the gating properties of $K_v7.2$.

In contrast, substitution at position R6 with either Q or W residues resulted in similar effects on $K_v7.2$ channel gating. In fact, both steady-state and kinetic properties of $K_v7.2$ channels carrying the R6Q or R6W substitution were indistinguishable, because the activation $V_{1/2}$, the slope factors *k*, and the activation time constants (125 ± 15 ms and 199 ± 42 ms for R6Q and R6W channels, respectively; n = 4–6) were identical in homomeric channels formed by R6Q or R6W subunits (Fig. 6).

DISCUSSION

$K_v7.2$ subunits participate to the formation of I_{KM}, a widespread regulator of neuronal excitability. Mutations in the $K_v7.2$ gene cause BFNS, a rare form of human epilepsy. Two BFNS-causing mutations in $K_v7.2$ affect positively charged residues (R207 and R214) in the S_4 segment, whose role in the voltage-sensing of K_v channels is firmly established. In agreement with this hypothesis, gating changes were described in $K_v7.2$ channels carrying such mutations (16,17). This study was undertaken to dissect the contribution of each of the six arginine residues present in the S_4 segment on the voltage-sensing of $K_v7.2$ channels. To this aim, each of these residues was substituted by glutamine residues, thus neutralizing the positive charge, and the functional properties of the mutant $K_v7.2$ channels were studied using whole-cell and single-channel patch-clamps upon their heterologous expression in CHO cells. The results suggest that each of the charged arginines in the S_4 segment of $K_v7.2$ subunits plays a significant role in voltage-dependent channel gating. Strikingly, neutralization of a single R at position 201 was sufficient to cause a significant loss of voltage dependence in channel activation.

None of the mutations investigated here impeded channel function. In contrast, neutralization of the residues corresponding to $K_v7.2$ positions R4 or R5 in *Shaker* (ShB) channels (25), and R4 in hyperpolarization-activated cyclic-nucleotide gated channels (HCN2) (26), did not produce functional homomeric channels, possibly because of altered subunit trafficking and folding, leading to greatly reduced surface expression (27). Interestingly, incorporation into a

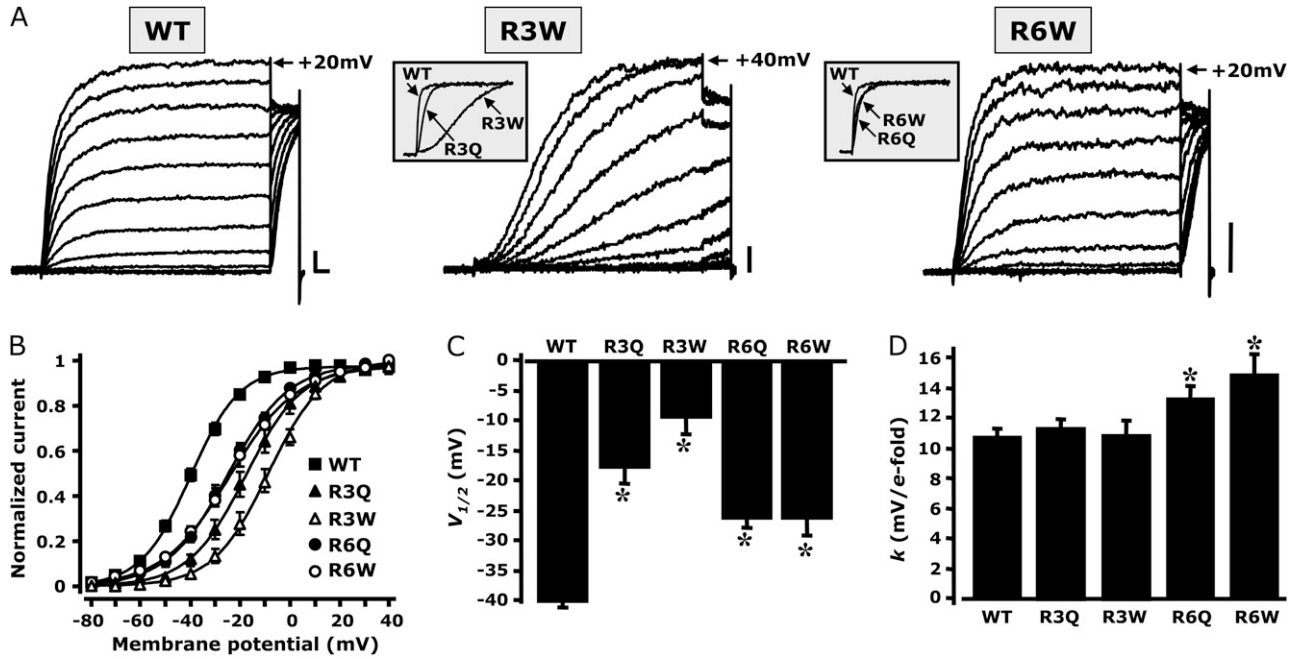

FIGURE 6 Comparison between gating properties of $K_v7.2$ channels carrying Q- or W-substituted R3 or R6 residues. (*A*) Representative current traces recorded using same voltage protocol described in Fig. 2. Insets, Comparisons of initial parts of normalized current traces at +20 mV for the indicated channels. (*B*) Steady-state activation curves, obtained by plotting normalized currents at the beginning of the 0-mV pulse as a function of the preceding conditioning potential. Continuous lines represent Boltzmann fits of the experimental data. $V_{1/2}$ (expressed in mV, *C*) and *k* (expressed in mV/*e*-fold, *D*) values were obtained for each indicated channel. *Values significantly different ($p < 0.05$) from corresponding value for wt$K_v7.2$ channels. Current scale, 200 pA; timescale, 0.2 s.

tetrameric concatenamer of the rat homologue of *Shaker* (rRCK1) of a single subunit carrying the mutation corresponding to $K_v7.2$ R4Q or R5Q recovered functional channels displaying a negative and positive shift in current activation properties, respectively (28).

Neutralization of each of the R residues caused significant effects on $K_v7.2$ channel gating. The most striking effect on voltage dependence was seen when the R2 residue was replaced by a glutamine. The currents carried by mutant R2Q $K_v7.2$ channels displayed largely time- and voltage-independent activation, and behaved like those carried by K^+-selective leak pores. Similar functional consequences on K^+ channel gating were previously obtained in other voltage-dependent channels upon substitution of positively charged R residues in S_4. However, in *Shaker* (ShB) channels, at least three residues, corresponding to $K_v7.2$ R1, R2, and R3, need to be neutralized simultaneously to produce such a dramatic effect (29). In addition, residues immediately before the S_4 segment were involved in the stabilization of the activated conformation of the voltage sensor. Thus, Tang and Papazian (30) found that in $K_v10.1$ channels, the introduction of a negatively charged amino acid two residues before the first R in the S_4 segment (A345E), a substitution which reproduced the sequence of the voltage-independent olfactory cyclic nucleotide gated channels, produced a significant negative shift in the steady-state voltage dependence of activation. Mutations affecting uncharged residues at this same position in $K_v7.2$ were recently found in BFNS families (31). Thus, in agreement with our findings that the R1Q mutation also increased the stability of the voltage-sensor conformation in the activated position at more negative voltages, these results suggest that the net charge of the region corresponding to the end of the S_3–S_4 linker and the N-terminal portion of S_4 is a crucial gating determinant in K_v channels. Thus, an increased positive net charge within this region is likely to stabilize the resting (closed) state of the voltage sensor, whereas the introduction of negative charges or the removal of positive charges favors the activated (open) conformation. Such conclusions also seem valid for $Na_v1.2$ voltage-dependent Na^+ channels, for which the removal of positive charges within the N-terminal half of S_4 produces negative shifts in the voltage dependence of activation, whereas more subtle and opposing effects are triggered by the neutralization of more distal positive charges (32). Moreover, direct gating-current measurements of the total gating-charge translocation in *Shaker* K^+ channels suggest that movement of the N-terminal half, but not of the C-terminal end, of the S_4 segment underlies gating currents (33).

The dramatic changes in voltage-dependent gating observed in macroscopic current recordings from R2Q mutant $K_v7.2$ channels were confirmed by our single-channel measurements, because mutant channels showed no significant change in p_o or shut and open time distributions between −80 and 0 mV. Moreover, our single-channel analysis also

showed that the maximal p_o, which is primarily determined by voltage-independent transitions between closed and open states, did not show statistically significant differences between wt and R2Q mutant $K_v7.2$ channels, again suggesting that the mutation dramatically affected the conformational changes occurring between the nonconducting closed states of the channels where most of the voltage-dependent transitions occur (34). Moreover, the similar maximal p_o of wt and R2Q $K_v7.2$ channels is consistent with the hypothesis that the maximal p_o of K_v7 channels is not determined by voltage, but by phosphatidylinositol 4,5-bisphosphate affinity, which is apparently not affected by the S_4 mutants described here (35). In addition to single-channel measurements, further support for the hypothesis that the R2Q mutation does not significantly change the open pore structure also derives from the identical TEA_e sensitivity and K^+ selectivity of wt and R2Q $K_v7.2$ channels.

As previously discussed, the functional consequences on voltage-dependent gating induced by the neutralization of R2 seem to be unique for $K_v7.2$ channels among other K_v channels. However, similar effects were also generated in the closely related cardiac $K_v7.1$ channels upon neutralizing the same R residue (R231A) (36). These authors interpreted such an effect as a consequence of the unique paucity of net charge present in the S_4 region of this channel (+3 in $K_v7.1$, whereas all other K_v7 members have +5). This view is supported by the formation of voltage-independent channels when $K_v7.4$ subunits carry a triple mutation (R207A, H216R, and Q220R), reproducing the net charge occurring in $K_v7.1$ subunits. However, our data suggest that the charge at the position corresponding to R2 has a primary role in stabilizing the resting conformation of the VSD, irrespective of the sequence of the C-terminal half of the S_4 segment because similar effects were produced by its neutralization in both $K_v7.1$ and $K_v7.2$ channels.

To test the role of charge removal versus steric hindrance at pathophysiologically relevant R3 and R6 sites in $K_v7.2$, we compared the functional properties of channels in which these positions were substituted by a Q (with a similar size to R, but missing the charge) or a W (a bulkier, uncharged amino acid). The results suggest that steric bulk plays a relevant role at position 207, but not at position 214, where the main functional effect of the mutations seems to be consequent to the loss of the charge. In fact, $K_v7.2$ R3W channels displayed a further positive shift in the half-activation potential when compared with R3Q channels, together with a marked slowing in current-activation kinetics. In contrast, both these parameters were identical in R6W and R6Q $K_v7.2$ channels. This result suggests that the skeletal muscle myokymia accompanying BFNS in patients carrying the R3W mutation may be caused by the specific introduction of the W residue at the R3 position (16). However, this view was challenged by the discovery of a novel family in which peripheral-nerve hyperexcitability with muscle myokymia was associated with an R3Q mutation in $K_v7.2$, in the apparent absence of other neurological symptoms, including BFNS (24). Several hypotheses can be proposed to explain the lack of BFNS in R3Q-carrying myokymic patients, including a different degree of heteromeric association with $K_v7.3$, a different subcellular localization of homomeric versus heteromeric channels in forebrain versus spinal motorneurons, and different degrees of dominant-negative suppression of I_{KM} function prompted by the two mutations at the R3 site. On the other hand, despite the obvious difficulties in drawing genotype-phenotype correlations based only on these functional results (37), the fact that the R6W mutation only caused small functional changes on $K_v7.2$ channel-gating is compatible with the fact that patients carrying such mutation are only affected by classic BFNS, with no other peripheral signs of neuronal hyperexcitability (17).

To provide further insights into the possible structural consequences of the replacement of the R3 residue with Q or W, and into the overall mechanism for the presumed effect of S_4 mutations on $K_v7.2$ channel VSD displacement during gating, we built a homology model of the $K_v7.2$ VSD. As a template, we used the crystal coordinates of the activated configuration of a recently described chimeric channel in which the voltage-sensor paddle (corresponding to the S_{3b}–S_4 region) of $K_v2.1$ was transferred into the $K_v1.2$ subunit (22) (PDB accession number 2R9R). The sequence identity between $K_v7.2$ and the $K_v1.2/2.1$ chimera is 29%. In this chimeric channel, it was proposed that the resting and activated positions of the VSD are stabilized by ionized hydrogen bonds between the charged R subunits in the S_4 segment and two negatively charged clusters: one facing the extracellular side of the membrane and provided by the S_1 and S_2 helices, and another closer to the intracellular membrane surface, involving the S_2 and the S_{3a} helices. The two clusters are separated by a highly conserved phenylalanine (F137) residue positioned in the middle of S_2 (the so-called ''phenylalanine gap''). As shown in Fig. 7 *A*, a similar spatial arrangement of charged residues within this region is evident from our $K_v7.2$ homology model. In particular, in the activated VSD configuration, R3 (R207) in $K_v7.2$ forms ionized hydrogen bonds with a negatively charged residue belonging to the external cluster (E130), whereas R4 (R210) is predicted to interact with negative charges of the inner cluster (E140 in S_2; D172 in S_3). Analysis of the model suggests that the replacement of R at position 207 with a neutral amino acid such as Q (Fig. 7 *B*) or W (Fig. 7 *C*) hampers this interaction. Thus, it seems plausible to hypothesize that in both R3Q and R3W channels, the activated configuration of the VSD is destabilized, explaining the positive shift in steady-state voltage dependence of activations observed in these mutants. Furthermore, as also suggested by biochemical experiments using cysteine-reacting methanethiosulfonate reagents in *Shaker* channels (38), the R3 residue in S_4 appears to flip up around the ''phenylalanine gap'' on its way across the membrane during the activation process (22). Therefore, it seems possible that the presence of a bulkier W at this position delays such movement more than the smaller Q residue,

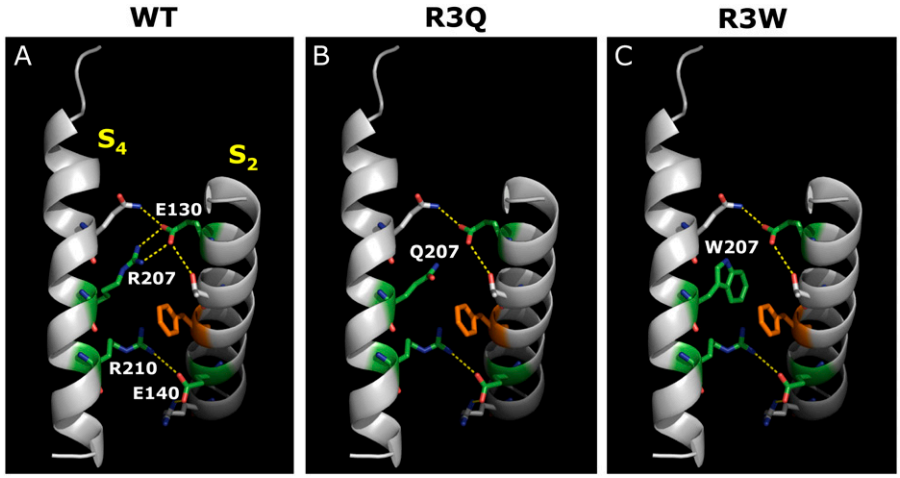

FIGURE 7 Three-dimensional homology model of $K_v7.2$ VSD. For clarity, only regions corresponding to the S_2 and S_4 segments are shown, as indicated. (*A*) wt$K_v7.2$ subunit. (*B*) R3Q mutant $K_v7.2$ subunit. (*C*) R3W mutant $K_v7.2$ subunit. The peptide backbone is shown as gray ribbons. Residues at positions E130 (in S_2) and R207 (in S_4) are shown in green. Ionized hydrogen bonds are highlighted in yellow, and the highly conserved phenylalanine residue in S_2 is shown in orange.

leading to a substantial slowing of R3W channel opening kinetics.

As previously pointed out, the R2Q substitution led to a significant destabilization of the resting VSD conformation. Although the available structures only reveal the VSD conformation in their active states, analysis of the $K_v1.2/2.1$ chimera suggests that in the resting VSD conformation, the R1 residue is positioned at the level of the ''phenylalanine gap'' (22). Therefore, one could speculate that the highly conserved R2 side chain positioned below R1 could interact with the negatively charged residues of the inner cluster, to stabilize the resting VSD conformation. Therefore, the R2Q substitution, by preventing such an interaction, would cause the VSD to be largely locked in a permanently activated position.

In conclusion, our data show that each charged residue in S_4 has a different role in voltage-dependent gating of $K_v7.2$ channels. The N-terminal residues are more involved in stabilizing the resting conformation, and the more distal residues are more involved in controlling the activated position of the voltage-sensor. This analysis does not allow for the definition of a precise mechanism of VSD dislocation during the activation process of $K_v7.2$ channels. Nevertheless, by highlighting the relative functional role of each R residue in channel gating, these results provide molecular clues about the pathophysiology of BFNS and possibly other neuropsychological abnormalities associated with $K_v7.2$ mutations.

We are deeply indebted to Prof. Thomas J. Jentsch, Department of Physiology and Pathology of Ion Transport, Leibniz-Institut für Molekulare Pharmakologie, Berlin-Buch, Germany, for $K_v7.2$ cDNA, and to Dr. Paolo Ambrosino, Department of Neuroscience, University of Naples, Naples, Italy, for help with $K_v7.2$ homology modeling.

This study was supported by grants from Telethon GP07125, by the European Commission Strategic Research Program No. 503038 and E-Rare 2007 to M.T., and by United States National Institutes of Health grant RO1 NS043394 and American Heart Association grant-in-aid 0755071Y to M.S.S.

REFERENCES

1. Hille, B. 2001. Ion Channels of Excitable Membranes. Sinauer Associates, Inc., Sunderland, MA.
2. Doyle, D. A., J. Morais Cabral, R. A. Pfuetzner, A. Kuo, J. M. Gulbis, S. L. Cohen, B. T. Chait, and R. MacKinnon. 1998. The structure of the potassium channel: molecular basis of K^+ conduction and selectivity. *Science*. 280:69–77.
3. Jiang, Y., A. Lee, J. Chen, M. Cadene, B. T. Chait, and R. MacKinnon. 2002. Crystal structure and mechanism of a calcium-gated potassium channel. *Nature*. 417:515–522.
4. Jiang, Y., A. Lee, J. Chen, M. Cadene, B. T. Chait, and R. MacKinnon. 2002. The open pore conformation of potassium channels. *Nature*. 417:523–526.
5. Kuo, A., J. M. Gulbis, J. F. Antcliff, T. Rahman, E. D. Lowe, J. Zimmer, J. Cuthbertson, F. M. Ashcroft, T. Ezaki, and D. A. Doyle. 2003. Crystal structure of the potassium channel KirBac1.1 in the closed state. *Science*. 300:1922–1926.
6. Bezanilla, F. 2000. The voltage sensor in voltage-dependent ion channels. *Physiol. Rev*. 80:555–592.
7. Yellen, G. 2002. The voltage-gated potassium channels and their relatives. *Nature*. 419:35–42.
8. Jiang, Y., A. Lee, J. Chen, V. Ruta, M. Cadene, B. T. Chait, and R. MacKinnon. 2003. X-ray structure of a voltage-dependent K^+ channel. *Nature*. 423:33–41.
9. Long, S. B., E. B. Campbell, and R. Mackinnon. 2005. Crystal structure of a mammalian voltage-dependent *Shaker* family K^+ channel. *Science*. 309:897–903.
10. Long, S. B., E. B. Campbell, and R. Mackinnon. 2005. Voltage sensor of Kv1.2: structural basis of electromechanical coupling. *Science*. 309: 903–908.
11. Tombola, F., M. M. Pathak, and E. Y. Isacoff. 2005. How far will you go to sense voltage? *Neuron*. 48:719–725.
12. Wang, H. S., Z. Pan, W. Shi, B. S. Brown, R. S. Wymore, I. S. Cohen, J. E. Dixon, and D. McKinnon. 1998. KCNQ2 and KCNQ3 potassium channel subunits: molecular correlates of the M-channel. *Science*. 282:1890–1893.
13. Brown, D. A., and P. R. Adams. 1980. Muscarinic suppression of a novel voltage-sensitive K^+ current in a vertebrate neurone. *Nature*. 283:673–676.
14. McNaughton-Smith, G. A. W. A. 2006. Compounds that activate KCNQ (2–5) family of potassium ion channels. *In* Voltage-Gated Ion Channels as Drug Targets Series: Methods and Principles in Medicinal Chemistry. C. M. Triggle, D. J. Rampe, W. Zheng, editors. Wiley-VCH Verlag GmbH & Co., Weinheim, Germany. 355–380.

15. Miceli, F., M. V. Soldovieri, M. Martire, and M. Taglialatela. 2008. Molecular pharmacology and therapeutic potential of neuronal Kv7-modulating drugs. *Curr. Opin. Pharmacol.* 8:65–74.

16. Dedek, K., B. Kunath, C. Kananura, U. Reuner, T. J. Jentsch, and O. K. Steinlein. 2001. Myokymia and neonatal epilepsy caused by a mutation in the voltage sensor of the KCNQ2 K^+ channel. *Proc. Natl. Acad. Sci. USA.* 98:12272–12277.

17. Castaldo, P., E. Miraglia del Giudice, G. Coppola, A. Pascotto, L. Annunziato, and M. Taglialatela. 2002. Benign familial neonatal convulsions caused by altered gating of KCNQ2/KCNQ3 potassium channels. *J. Neurosci.* 22:RC199 (1–6).

18. Selyanko, A. A., J. K. Hadley, and D. A. Brown. 2001. Properties of single M-type KCNQ2/KCNQ3 potassium channels expressed in mammalian cells. *J. Physiol.* 534:15–24.

19. Li, Y., N. Gamper, and M. S. Shapiro. 2004. Single-channel analysis of KCNQ K^+ channels reveals the mechanism of augmentation by a cysteine-modifying reagent. *J. Neurosci.* 24:5079–5090.

20. Colquhoun, D., and A. G. Hawkes. 1995. The principles of the stochastic interpretation of ion-channel mechanisms. *In* Single-Channel Recording. B. Sakmann and E. Neher, editors. Plenum Press, New York 589–633.

21. Schwede, T., J. Kopp, N. Guex, and M. C. Peitsch. 2003. SWISS-MODEL: an automated protein homology-modeling server. *Nucleic Acids Res.* 31:3381–3385.

22. Long, S. B., X. Tao, E. B. Campbell, and R. MacKinnon. 2007. Atomic structure of a voltage-dependent K^+ channel in a lipid membrane-like environment. *Nature.* 450:376–382.

23. Simmons, M. A., and C. R. Schneider. 1998. Regulation of M-type potassium current by intracellular nucleotide phosphates. *J. Neurosci.* 18:6254–6260.

24. Wuttke, T. V., K. Jurkat-Rott, W. Paulus, M. Garncarek, F. Lehmann-Horn, and H. Lerche. 2007. Peripheral nerve hyperexcitability due to dominant-negative KCNQ2 mutations. *Neurology.* 69:2045–2053.

25. Papazian, D. M., L. C. Timpe, Y. N. Jan, and L. Y. Jan. 1991. Alteration of voltage-dependence of *Shaker* potassium channel by mutations in the S4 sequence. *Nature.* 349:305–310.

26. Chen, S., J. Wang, L. Zhou, M. S. George, and S. A. Siegelbaum. 2007. Voltage sensor movement and cAMP binding allosterically regulate an inherently voltage-independent closed-open transition in HCN channels. *J. Gen. Physiol.* 129:175–188.

27. Papazian, D. M., X. M. Shao, S. A. Seoh, A. F. Mock, Y. Huang, and D. H. Wainstock. 1995. Electrostatic interactions of S4 voltage sensor in *Shaker* K^+ channel. *Neuron.* 14:1293–1301.

28. Tytgat, J., K. Nakazawa, A. Gross, and P. Hess. 1993. Pursuing the voltage sensor of a voltage-gated mammalian potassium channel. *J. Biol. Chem.* 268:23777–23779.

29. Bao, H., A. Hakeem, M. Henteleff, J. G. Starkus, and M. D. Rayner. 1999. Voltage-insensitive gating after charge-neutralizing mutations in the S4 segment of *Shaker* channels. *J. Gen. Physiol.* 113:139–151.

30. Tang, C. Y., and D. M. Papazian. 1997. Transfer of voltage independence from a rat olfactory channel to the *Drosophila* ether-a-go-go K^+ channel. *J. Gen. Physiol.* 109:301–311.

31. Soldovieri, M. V., M. R. Cilio, F. Miceli, G. Bellini, E. Miraglia del Giudice, P. Castaldo, C. C. Hernandez, M. S. Shapiro, A. Pascotto, L. Annunziato, and M. Taglialatela. 2007. Atypical gating of M-type potassium channels conferred by mutations in uncharged residues in the S4 region of KCNQ2 causing benign familial neonatal convulsions. *J. Neurosci.* 27:4919–4928.

32. Stuhmer, W., F. Conti, H. Suzuki, X. D. Wang, M. Noda, N. Yahagi, H. Kubo, and S. Numa. 1989. Structural parts involved in activation and inactivation of the sodium channel. *Nature.* 339:597–603.

33. Aggarwal, S. K., and R. MacKinnon. 1996. Contribution of the S4 segment to gating charge in the Shaker K+ channel. *Neuron.* 16:1169–1177.

34. Zagotta, W. N., and R. W. Aldrich. 1990. Alterations in activation gating of single *Shaker* A-type potassium channels by the Sh5 mutation. *J. Neurosci.* 10:1799–1810.

35. Li, Y., N. Gamper, D. W. Hilgemann, and M. S. Shapiro. 2005. Regulation of Kv7 (KCNQ) K^+ channel open probability by phosphatidylinositol 4,5-bisphosphate. *J. Neurosci.* 25:9825–9835.

36. Panaghie, G., and G. W. Abbott. 2007. The role of S4 charges in voltage-dependent and voltage-independent KCNQ1 potassium channel complexes. *J. Gen. Physiol.* 129:121–133.

37. Soldovieri, M. V., F. Miceli, G. Bellini, G. Coppola, A. Pascotto, and M. Taglialatela. 2007. Correlating the clinical and genetic features of benign familial neonatal seizures (BFNS) with the functional consequences of underlying mutations. *Channels.* 1:228–233.

38. Larsson, H. P., O. S. Baker, D. S. Dhillon, and E. Y. Isacoff. 1996. Transmembrane movement of the shaker K^+ channel S4. *Neuron.* 16: 387–397.